NORSAR Scientific Report No. 1-2006

Semiannual Technical Summary

1 July - 31 December 2005

Frode Ringdal (ed.)

Kjeller, January 2006

6.5 Moment tensor (MT) inversion for regional events in Fennoscandia and adjacent areas

6.5.1 Introduction

The reliable determination of earthquake epicenters and focal mechanisms, *i.e.*, centroid moment tensor solutions, is an important objective of earthquake seismology. Centroid moment tensors are fundamental input data for fast hazard estimation of aftershocks, quantitative simulation of tsunamis in case of submarine earthquakes, and seismo-tectonic evaluation and creation of seismic hazard maps.

Although moment tensor (MT) inversion is routinely applied by miscellaneous institutions for teleseismic events, it is rarely exerted in the case of weaker regional events with magnitudes of about 4.0. The reason for this is that regional earthquakes possess higher frequencies and reliable regional velocity models of the crust and upper mantle are required (Bruhns, 2003).

T. Dahm (University of Hamburg) and F. Krüger (University of Potsdam) developed algorithms to accomplish robust MT inversions for regional events with magnitudes of 4.0 – 4.5 (Dahm *et al.*, 1999; Dahm & Krüger, 1999; Krüger & Dahm, 2002). In this study, we applied these programs to regional earthquakes observed in Fennoscandia.

6.5.2 Moment tensor theory

During MT inversion, the focus lies on the information that data provide about earthquake mechanisms. The location of the earthquake as well as the focal time are assumed to be known. Amplitudes and shape of radiated waves depend on kinematics of faulting, and reflect the geometry of the fault and the motion on it. The concept is to model seismic waves generated by an earthquake by solving the equation of motion with faulting represented as equivalent body forces that result in the same seismic radiation pattern (Stein & Wysession, 2003). A seismic MT is a general concept, describing in a first order approximation the equivalent forces of a variety of seismic point sources (Jost & Herrmann, 1989).

The first MT inversions (calculation of MT elements from observed seismograms) were conducted by Gilbert (1973) in the frequency domain using the linearity between MT and Green's function elements. The concept of seismic MTs was taken up by Backus & Mulcahy (1976) and Backus (1977a, 1977b). An overview is given by Jost & Herrmann (1989).

In the far-field, ground motion displacement $\vec{u}$ can be expressed as (see *e.g.*, Dahm *et al.*, 2004):

$$u_n(\vec{x}, t) = \int_0^\infty M_{pq}(t) \frac{\delta}{\delta \xi_q} G_{np}(\vec{x}, t-\tau; \vec{\xi}, 0) d\tau \ , \qquad (1)$$

where $\vec{x}$ is pointing to the station, $\vec{\xi}$ is directed towards the moment centroid in the origin of the coordinate system and G_{np} is the *n*-th component of ground movement at the station in response to a unit-force excitation in *p*-direction at the source (a Green's function).

M_{pq} is no longer time-dependent if a step function is assumed as source time function.

Further, it holds that

$$\frac{\delta}{\delta\xi_q} G_{np}(\vec{x}, T) = \frac{\delta G_{np}}{\delta x_j}\frac{\delta x_j}{\delta\xi_q} + \frac{\delta G_{np}}{\delta t}\frac{\delta T}{\delta\xi_q} \tag{2}$$

with the retardation time $T = t - \frac{r}{c}$, including $r = \sqrt{(x_1-\xi_1)^2 + (x_2-\xi_2)^2 + (x_3-\xi_3)^2}$, and c being the wave velocity. The first part of Equ. (2) can be neglected in the far-field, thus leaving

$$u_n(\vec{x}, t) \approx M_{pq}\int_0^\infty \dot{G}_{np}(\vec{x}, t-\tau)\frac{\delta T}{\delta\xi_q}d\tau = M_{pq}G_{np}(\vec{x}, t)\frac{\delta T}{d\xi_q}, \tag{3}$$

which can be used to infer radiation patterns for a general MT source.

The meaning of a MT is clearest when examining its eigenvalues and eigenvectors in the principal axis transformation (Jost & Herrmann, 1989; Dahm *et al.*, 2004):

$$M = \begin{bmatrix} a_{1x} & a_{2x} & a_{3x} \\ a_{1y} & a_{2y} & a_{3y} \\ a_{1z} & a_{2z} & a_{3z} \end{bmatrix} \begin{bmatrix} e_1 & 0 & 0 \\ 0 & e_2 & 0 \\ 0 & 0 & e_3 \end{bmatrix} \begin{bmatrix} a_{1x} & a_{1y} & a_{1z} \\ a_{2x} & a_{2y} & a_{2z} \\ a_{3x} & a_{3y} & a_{3z} \end{bmatrix}, \tag{4}$$

where a_i is the orthonormal eigenvector to the eigenvalue e_i. The eigenvalues e'_i of the deviatoric MT are defined by $e'_i = e_i - tr$ with the trace $tr = \frac{e_1 + e_2 + e_3}{3}$.

Assuming that $|e'_3| \geq |e'_1| \geq |e'_2|$, the MT can be decomposed in the following way:

$$\begin{bmatrix} e_1 & 0 & 0 \\ 0 & e_2 & 0 \\ 0 & 0 & e_3 \end{bmatrix} = tr \underbrace{\begin{bmatrix} 1 & 0 & 0 \\ 0 & 1 & 0 \\ 0 & 0 & 1 \end{bmatrix}}_{\text{isotropic}} + (e_1 - e_2) \underbrace{\begin{bmatrix} 1 & 0 & 0 \\ 0 & 0 & 0 \\ 0 & 0 & -1 \end{bmatrix}}_{\text{dev.: best DC}} + (e_2 - tr) \underbrace{\begin{bmatrix} 1 & 0 & 0 \\ 0 & 1 & 0 \\ 0 & 0 & -2 \end{bmatrix}}_{\text{dev.: CLVD}}. \tag{5}$$

The sum of the eigenvalues is related to the volume change in the source (isotropic part). If it is zero, only the deviatoric part exists. It represents a pure double couple (DC) source, if one of the eigenvalues vanishes. If this is not the case, the deviatoric MT can be decomposed either after Kanamori & Given (1981) into a major and minor DC or after Knopoff & Randall (1970) into a DC and a compensated linear vector dipole (CLVD).

Often, the minor DC or the CLVD reflect lateral heterogeneities in the Earth, noise in the data and the deviation of the earthquake from a point source, but in some cases, it may result from physical conditions as simultaneous ruptures on nearby faults with different orientations. Sources with large CLVD components have been observed in several complicated tectonic environments, *e.g.*, volcanic areas (Stein & Wysession, 2003).

Equ. (3) can be written in the simple matrix form (*e.g.*, Dahm *et al.*, 2004):

$$\vec{u} = \boldsymbol{GM} \tag{6}$$

which in time domain results in the linear inversion

$$\boldsymbol{m} = \boldsymbol{G}^{-1}\vec{u} \tag{7}$$

where $\boldsymbol{G}^{-1}$ is the generalized inverse. In frequency domain, the inversion becomes nonlinear due to the nonlinear dependence of the observed amplitude spectra on the MT elements. Equations have to be linearized by Taylor series expansions around a starting solution and iterative inversion schemes have to be used. The same holds true for certain constraints on the MT, *e.g.*, a constraint to a DC or a tensile crack.

Since the focal depth is not very well constrained, inversions can be performed for several depths, where the most probable depth will minimize the quadratic error between observed and theoretical waveforms, since differences in source depth influence the relative excitation of normal modes (Jost & Herrmann, 1989). The connection between source depth and results of MT inversion was analyzed by Sipkin (1982).

6.5.3 Program package MTINVERS

A program package called MTINVERS has been developed to perform MT inversion. The work steps include data pre-processing, picking of phases, calculation of Green's functions and finally the amplitude spectra inversion and inversion in time domain. The Green's functions are calculated applying the reflectivity code *refgreen* by Ungerer (1990). The program for MT inversion *mtinvers* has been provided by T. Dahm (University of Hamburg) and F. Krüger (University of Potsdam). A description of the code is given in Dahm *et al.* (2004). Seismic data processing is done using *EP* (Fyen, 2004). C-shell scripts and Fortran programs are employed as intermediary steps between codes, to construct input files and to direct the program flow.

Thus, the user has to fill in only one input file (called *input.list*) and to run only one script file (*input.csh*) to perform the whole process. Additionally, routines to test filtering and resampling have been developed along with GMT scripts (Wessel & Smith, 2003) for plotting of results and documentation has been prepared. Input parameters are:

For the pre-processing:

- time and location of earthquake, length of data extraction, filter parameters and sampling rate for body and surface waves individually

For the calculation of Green's functions:

- velocity model, depth range, slowness range, duration of earthquake as well as frequency range, sampling rate (same as for data) and number of integration points for body and surface waves individually

For the amplitude spectra inversion:

- inversion constraints, taper window, weight with distance and possibly a restricted frequency range for body and surface waves individually

For the inversion in time domain:

- depth of earthquake (result of amplitude spectra inversion).

Data pre-processing comprises broadband filtering, restitution to ground motion, resampling and rotation in 2-D. In principle, all kinds of phases can be picked. We confined the search to P-, SV-, SH-, Rayleigh and Love waves (P- and Rayleigh wave on vertical (z) component, SV- and Rayleigh wave on the radial (r) component and SH- and Love wave on the transverse (t)

component). Green's functions are calculated by the reflectivity method (e.g., Müller, 1985) in form of 8 elementary seismograms for z, r and t components. They are determined for a whole depth range, which is conserved for amplitude spectra inversion and only restricted to one depth during inversion in time domain by searching for the lowest misfit between observed and synthetic seismograms during amplitude spectra inversion. Other indicators for a stable solution can be a high DC percentage and the visual comparison of observed and calculated amplitude spectra and seismograms. After time domain inversion, the resulting MT is decomposed in isotropic and deviatoric parts. The deviatoric part is further split in best DC and CLVD.

Both amplitude spectra inversion and inversion in time domain have some assets and drawbacks. Amplitude spectra inversion is more complicated in a mathematical sense, since equations are non-linear. Further, since no phase information is used, the method cannot distinguish between compressive and dilatational quadrants. On the other hand, amplitude spectra inversion is more stable than time domain inversion if the data are not yet aligned to the synthetic seismograms and it is also more stable in the cases of wrong velocity models or source depths. Since time domain inversion is less stable for high frequencies, it is also less stable for inversion of body waves. Many institutes which routinely apply MT inversions use only surface waves for inversions in the time domain or filter the signal at very low frequencies. For the inversion of regional events as presented here, the frequency content is generally higher and cannot be neglected.

When using data from a broadband array, the automatic processing routine treats each array station individually and a weighting factor can be introduced before inversion. Additionally, it is possible to calculate the beam manually and insert it as a seismogram pretending that it comes from a single station. The first case is suitable for the NORSAR array where the interstation distance is large enough to record differences in waveforms (especially for the 07 April 2004 Flisa event), the second approach can be used for the Spitsbergen array to enhance the signal-to-noise ratio. Until now, only the first approach has been applied.

In the following, results of the application of the MT inversion in amplitude and time domain to regional events are presented. Since the focus lies on testing of the method, only little or no interpretation of the MT solutions is given.

6.5.4 Results

Observed seismograms and theoretically calculated Green's functions are strongly depending on the velocity structure seen by the seismic waves. In Fig. 6.5.1, the different velocity models applied in this study are plotted and the PREM model is shown for comparison.

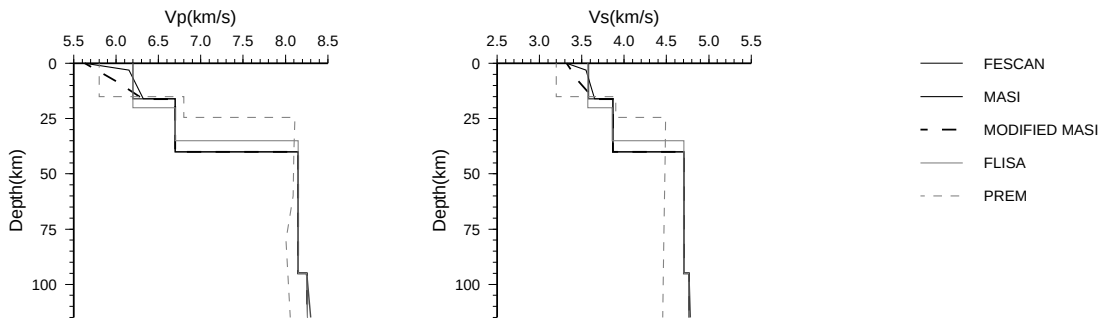

Fig. 6.5.1. Velocity models applied in this study.

At first, Green's functions have been calculated according to the standard velocity model used at NORSAR (FESCAN). Since this model does not sufficiently reproduce the surface wave dispersion, the MASI model by Roth & Bungum (2003) was also tested. Results were satisfactory for the Svalbard event, but not for the Jan Mayen event. Therefore, the MODIFIED MASI model was developed by trial-and-error resulting in lower velocity gradients in the upper crust. For the Flisa event, the velocity model by Schweitzer (2005) is used. The depth extent of the models is larger than displayed in Fig. 6.5.1.

The 14 April 2004 Jan Mayen earthquake

The 14 April 2004 Jan Mayen earthquake as well as the 04 July 2003 Svalbard earthquake were used for calibration of the parameters used during the calculation of Green's functions and inversion, especially the velocity models. The Jan Mayen event has a magnitude of Mw= 5.9 (HRVD, Harvard CMT catalog, 1998) and the epicenter is located at 7.747˚W and 71.067˚N. Fig. 6.5.2 shows the epicenter as a black star and the stations, which recorded data (APZ9, ARE0, FIA1, HFC2, KBS, NOA, and VSU), are shown as as grey triangles to give an impression of the azimuthal coverage.

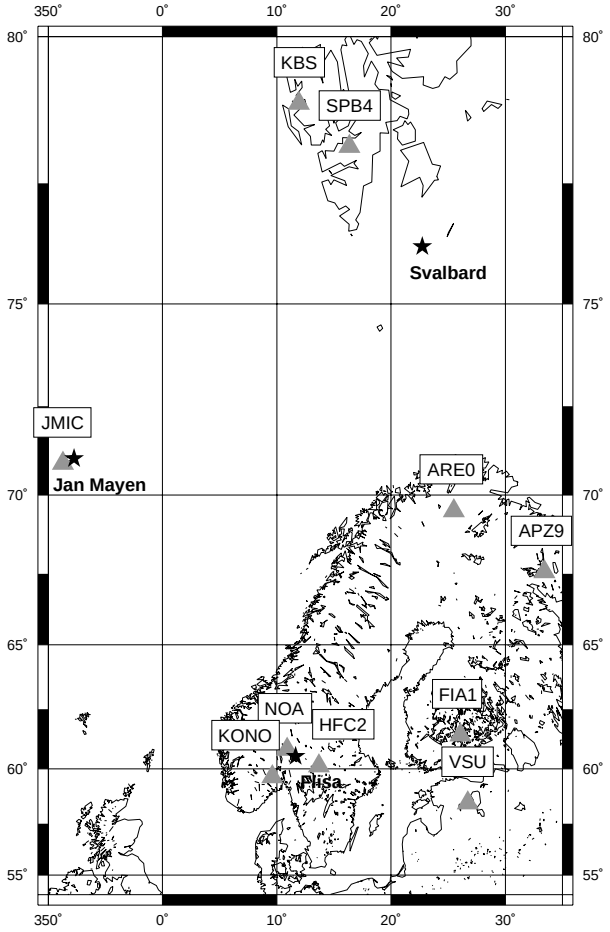

Fig. 6.5.2. Epicenters of the investigated earthquakes (Jan Mayen, Svalbard and Flisa) are shown as black stars and seismic stations (arrays) for which data have been used in this study are shown as grey triangles.

Fig. 6.5.3 shows the broadband filtered, restituted, resampled and rotated data as used in the inversion process; the filter parameters were chosen according to the surface wave analysis.

For the amplitude spectra inversion, the whole frequency range of 0.01 – 0.3 Hz was used for body waves and 0.01 – 0.07 Hz for surface waves, respectively. The MASI velocity model was used for the calculation of Green's functions, since the firstly applied FESCAN model proved inappropriate to excite surface waves sufficiently. The inversion results are displayed in Fig. 6.5.4 for a depth range from 2 to 8 km. Isotropic and DC percentage are of the same order for all depths, but the focal solution is rotated slightly and the misfit has a clear minimum at a depth of 5 km.

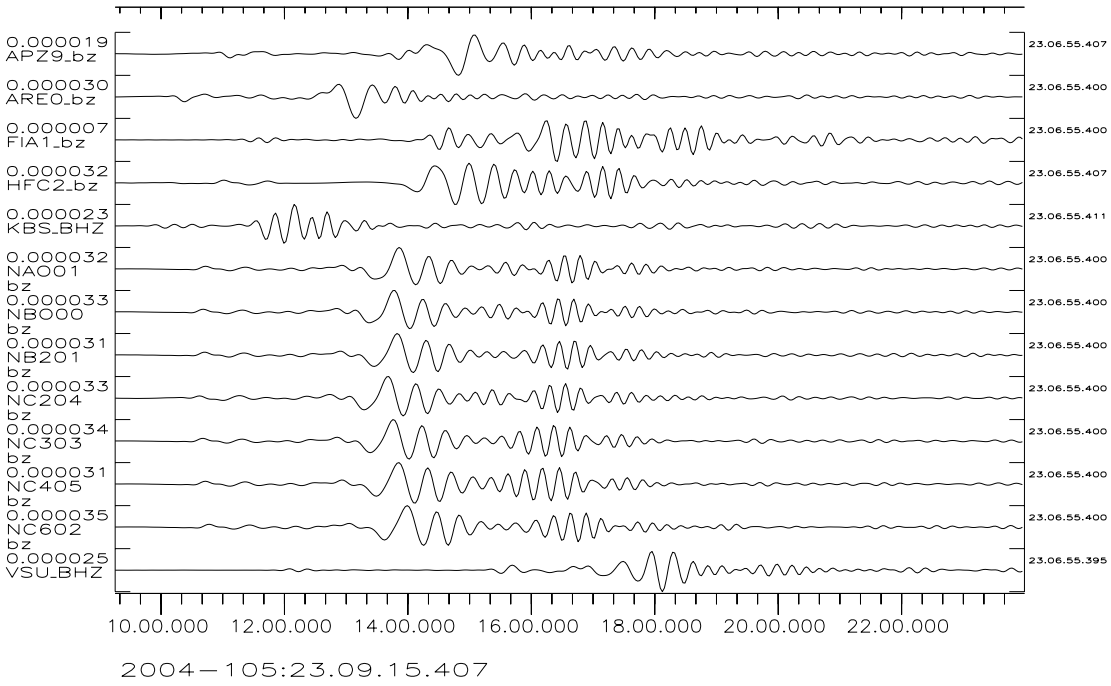

Fig. 6.5.3. Broadband filtered, restituted, resampled and rotated data; the data are prepared for surface wave analysis (filtered by 0.01 – 0.07 Hz); only z components are displayed.

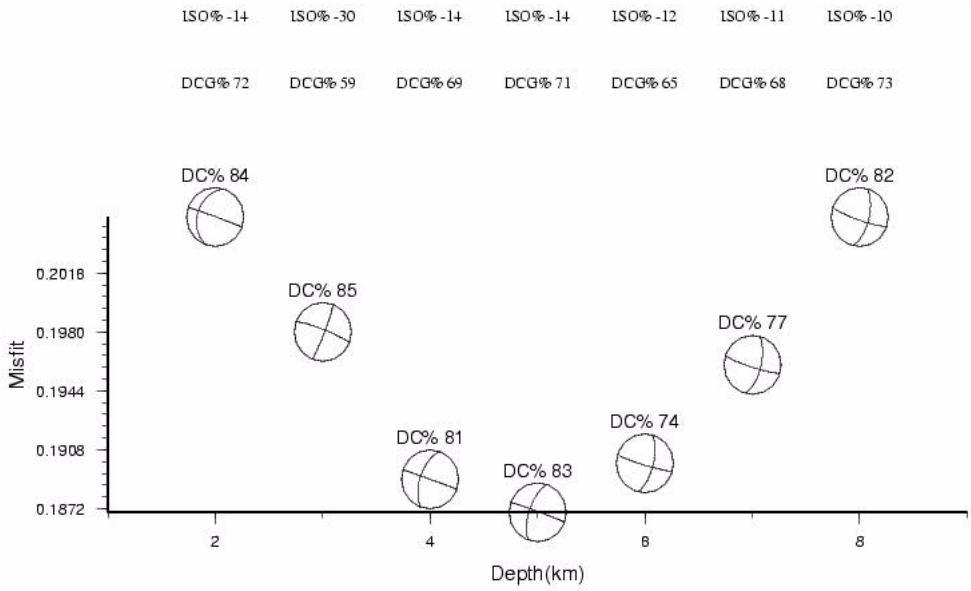

Fig. 6.5.4. Results of the amplitude spectra inversion: misfit and focal solutions for different depths.

The inversion in time domain was carried out in three steps of increasing frequency content. At first, body waves were filtered prior to inversion at 0.01 – 0.05 Hz and surface waves at 0.01 – 0.03 Hz, resulting in a misfit of 0.220. Next, the body wave frequency range amounted to 0.01-0.15 and the surface frequency range to 0.01 – 0.05 Hz with a misfit of 0.428. Finally, the frequency content covered the whole range of the pre-processed data between 0.01 – 0.3 Hz for body waves and 0.01 – 0.07 Hz for surface waves, yielding a misfit of 0.579.

In Fig. 6.5.5, the deviatoric MT and DC produced by MTINVERS are compared to the solutions of Harvard (HRVD, Harvard CMT catalog, 1998) and ETH Zürich (ZUR_RMT, Bernardi *et al.*, 2004), respectively. Further parameters produced by the MT inversion are listed in Table 6.5.1.

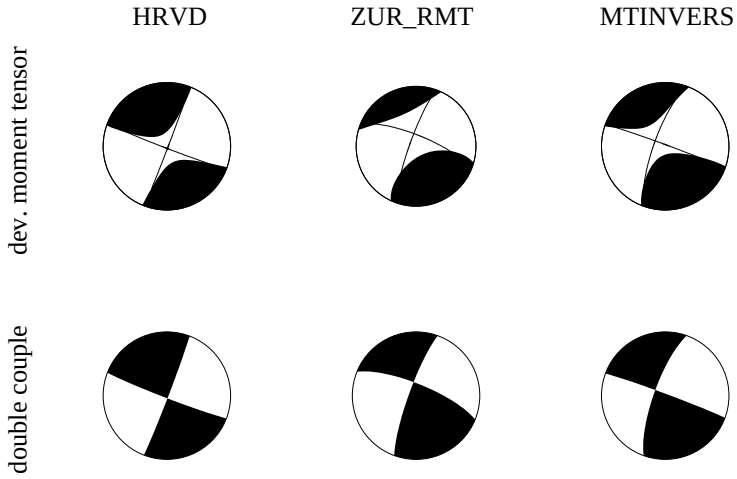

Fig. 6.5.5. Comparison of the deviatoric MTs (top) and DC parts (bottom) of the investigated Jan Mayen event as inverted with MTINVERS and as published by Harvard (Harvard CMT catalog, 1998) and ETH Zürich (Bernardi et al., 2004).

Table 6.5.1. Seismic moment, focal depth and fault plane solution as derived by MTINVERS and as published by Harvard (Harvard CMT catalog, 1998) and ETH Zürich (Bernardi *et al.*, 2004).

	HRVD	ZUR_RMT	MTINVERS
M0 (Nm)	7.90E+17	1.00E+18	3.40E+17
Depth (km)	12	12	5
Strike 1	111	200	199.8
Dip 1	87	81	75.7
Rake 1	2	165	177.6
Strike 2	21	292	290.4
Dip 2	88	75	87.6
Rake 2	177	9	14.3

Although the misfit provided by MTINVERS is rather high, the agreement between MT and the solutions determined by Harvard and ETH Zürich is good, the MTINVERS solutions for deviatoric MT and DC giving the visual impression of lying between the other two. The focal depth (given in Table 6.5.1) differs, but is still in the same range. The isotropic part amounts to 15%, the DC percentage is 70%.

The fit between observed and synthetic seismograms can be seen in Fig. 6.5.6. The MT solution in Fig. 6.5.5 was assumed as source signal. On the left, body wave cutouts are presented, surface waves cutouts are visible on the right. Time scales (in samples) are the same for each column. Columns from left to right show phases from the vertical, radial and transverse com-

ponent. Unfortunately, no body waves were detected on the transverse component. Observed data are plotted by black lines, calculated seismograms are displayed as grey lines. Stations and maximum amplitudes are indicated for each trace.

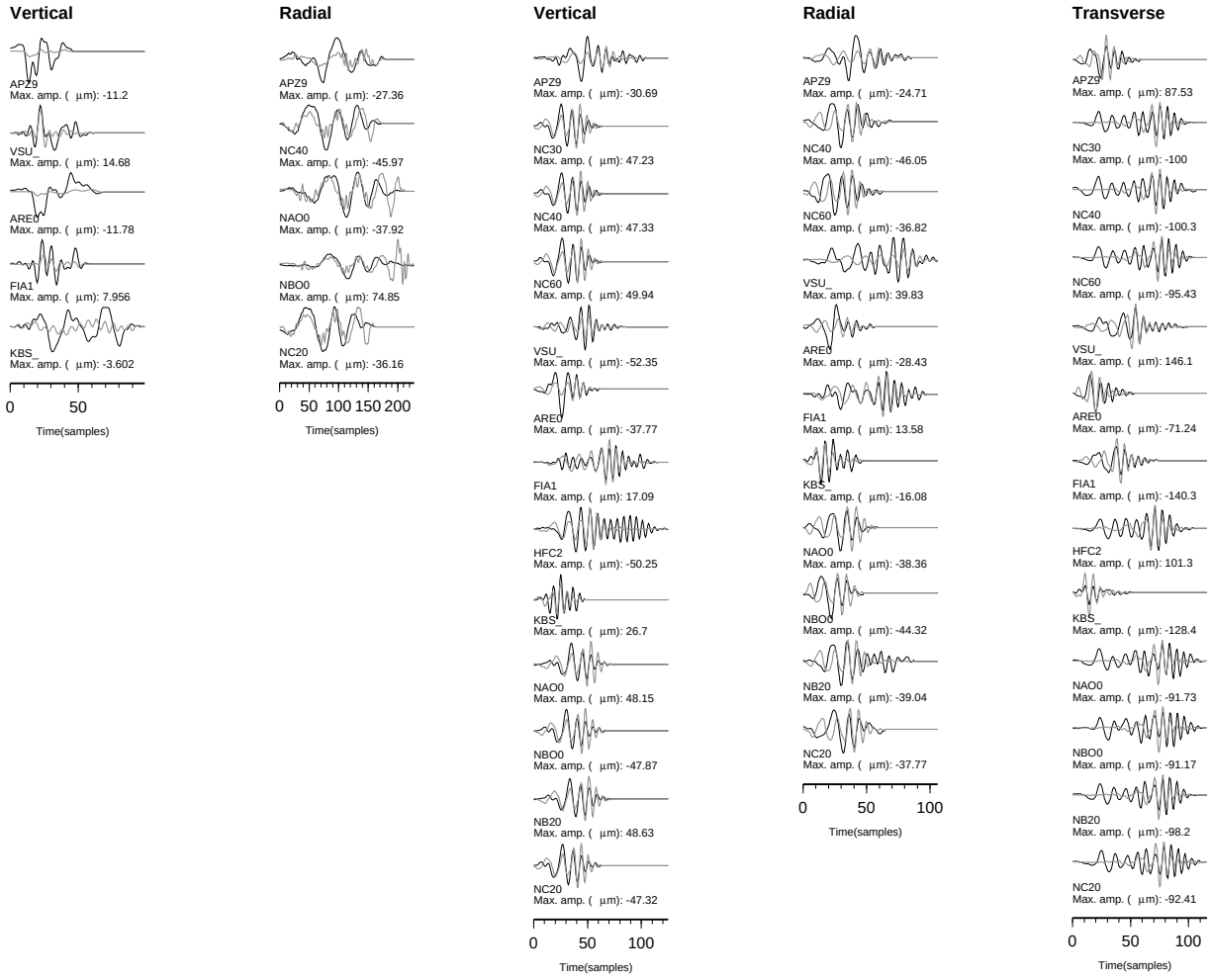

Fig. 6.5.6. Fit between observed data (black lines) and synthetic seismograms (grey lines) with the MT source assumed as in Fig. 6.5.5; left: body waves, right: surface waves.

Surface wave fits are much better than body wave fits, since lower frequencies were used for inversion. Nevertheless, the seismograms are approximated sufficiently in most of the body wave cases, even if the observed seismograms are smoother. The poor fit at station KBS can be explained by the fact that in this case the seismic waves propagate exclusively through an oceanic crust and uppermost mantle, whereas the velocity model is designed for a continental crust and uppermost mantle. Synthetic seismograms at stations APZ9 and ARE0 also differ from the observations, but agree very well at the NORSAR array.

The 04 July 2003 Svalbard event

The second event used for calibration is the 04 July 2003 Svalbard event with a magnitude of Mw = 5.4 (HRVD, Harvard CMT catalog, 1998). Its location is at 22.745˚E and 76.253˚N. The azimuthal coverage with recording broadband stations (APZ9, ARE0, FIA1, HFC2, JMI, KBS, KONO, and NOA) is better than in the case of the Jan Mayen event, where all stations were situated east of the epicenter (see Fig. 6.5.2). The pre-processed data shown (Fig. 6.5.7) are filtered with parameters, suitably chosen for body wave analysis.

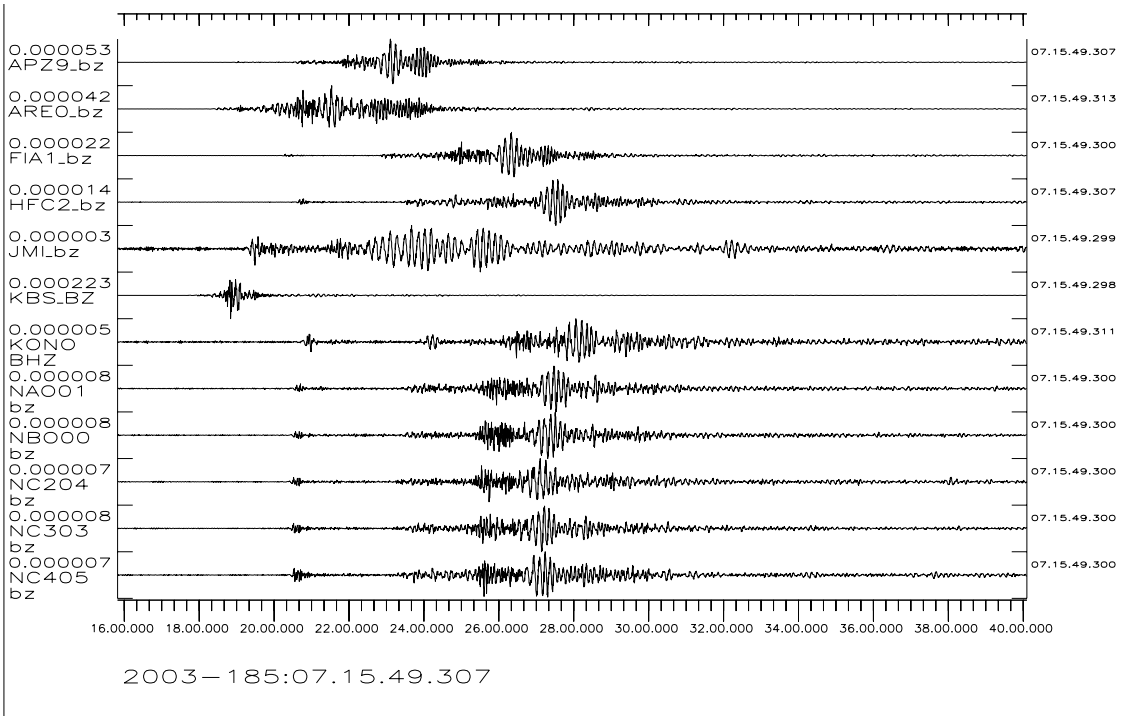

Fig. 6.5.7. Broadband filtered, restituted, resampled and rotated data; data are prepared for body wave analysis (filtered by 0.1 – 0.5 Hz); only vertical components are displayed.

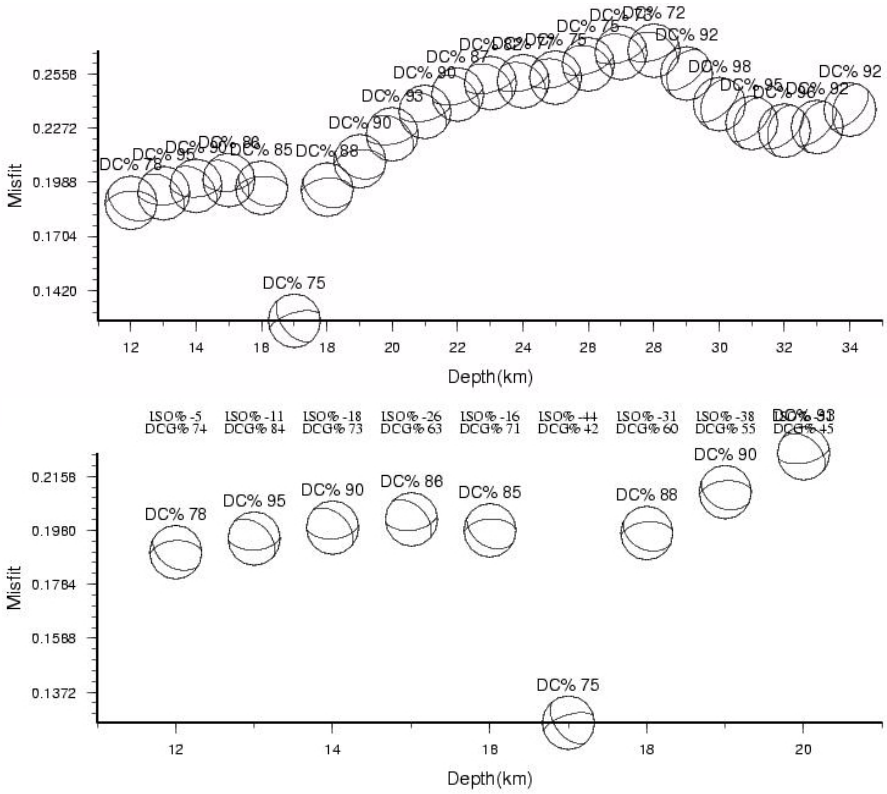

Fig. 6.5.8. Results of amplitude spectra inversion: misfit and focal solution plotted against depth; the bottom picture is a cutout of upper graphic.

In contrast to the Jan Mayen event, only higher frequencies could be used for body wave analysis (0.1 – 0.5 Hz) for the Svalbard event, whereas the frequency range used for surface waves is similar (0.01 – 0.05 Hz). Since the hypocenter depth has been calculated to be 33 ± 13 km by Stange & Schweitzer (2004), amplitude spectra inversions were computed for a broad depth range from 10 – 60 km. As can be seen in Fig. 6.5.8, the misfit increases towards higher depths, although a second minimum can be detected around 32 km. However, all solutions in the depth range of 12 – 20 km are quite similar (exept for some rotation) but a clear minimum can be found at a depth of 17 km, even if featuring a smaller DC percentage.

For inversion in the time domain, the following filter steps were applied: a) 0.1 – 0.23 Hz for body and 0.01 – 0.023 Hz for surface waves, b) 0.1 – 0.36 Hz for body and 0.01 – 0.036 for surface waves and c) 0.1 – 0.5 Hz for body and 0.01 – 0.05 Hz for surface waves, resulting in misfits of 0.240, 0.291 and 0.342 respectively, which is better than the misfit obtained for the Jan Mayen event. To successfully model the surface-wave dispersion, Green's functions were calculated by using the modified MASI model (Fig. 6.5.1). Both the deviatoric MT and the DC are presented in Fig. 6.5.9 for comparison with solutions from Harvard (Harvard CMT catalog, 1998) and ETH Zürich (Bernardi *et al.*, 2004). Table 6.5.2 provides all parameter values.

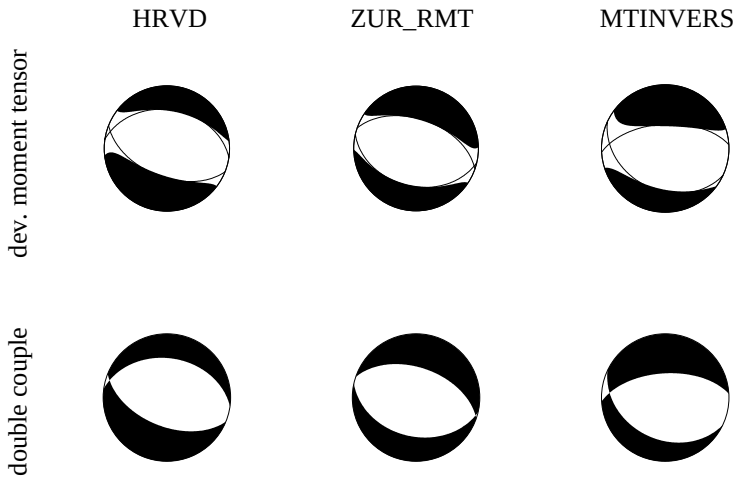

Fig. 6.5.9. Comparison of the deviatoric MTs (top) and DC parts (bottom) of the investigated Svalbard event as inverted with MTINVERS and as published by Harvard (Harvard CMT catalog, 1998) and ETH Zürich (Bernardi et al., 2004).

Table 6.5.2. Comparison of seismic moment, focal depth and fault plane solution produced by MTINVERS with results from Harvard and ETH Zürich.

	HRVD	ZUR_RMT	MTINVERS
M0 (Nm)	2.20E+17	1.80E+17	1.30E+17
Depth (km)	15	15	17
Strike 1	278	289	266.6
Dip 1	38	51	58.7
Rake 1	-101	-86	-105.9
Strike 2	112	103	115.2
Dip 2	53	39	34.8
Rake 2	82	-95	-65.8

The solutions are very similar, but the deviatoric tensor and the DC computed by MTINVERS are a little bit rotated. The depth is consistent and the seismic moment is in the same order of magnitude. The isotropic part amounts to 37% of the complete MT, the DC percentage is only

59%. The parameter "DC percentage" should not be overrated, since it is not well resolved by this type of inversion. The hypocentral depth of 17 km is probable, since Stange & Schweitzer (2004) state that recorded seismograms indicate a hypocenter within the crust. The fit between the observed data and synthetic seismograms is displayed in Fig. 6.5.10. In the surface wave frequency range, the fit between observed and calculated seismograms is extraordinarily good. Even for the high frequency body waves, the similarity is high. Synthetic seismograms and observations disagree the most at stations ARE0, JMI, KBS and SPB4.

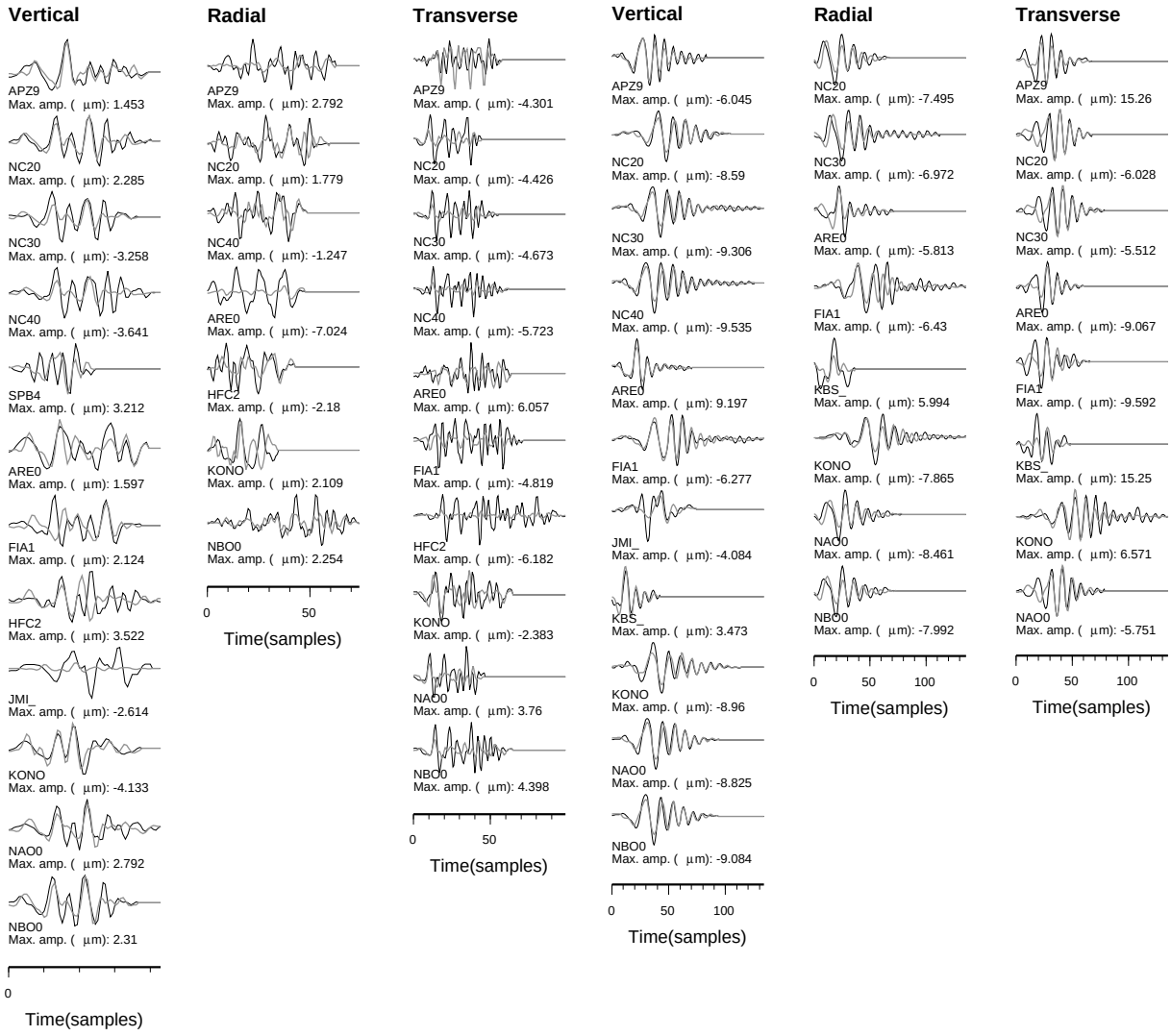

Fig. 6.5.10. Fit between observed data (black lines) and synthetic seismograms (grey lines) with MT source assumed as in Fig. 6.5.9; left: body waves, right: surface waves.

The 07 April 2004 Flisa event

The 07 April 2004 Flisa event affords the unusual opportunity to analyze an event occurring close to the NORSAR array with a magnitude of 3.5. The closest epicentral distance is less than 20 km. Its coordinates were 11.6526˚E and 60.5511˚N (Schweitzer, 2005; Fig. 6.5.11). The azimuthal coverage is enhanced by the recordings of station HFS. Because of the proximity to the epicenter, no surface waves can be observed (Fig. 6.5.12).

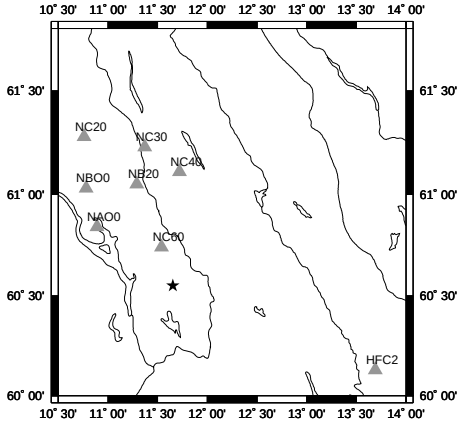

Fig. 6.5.11. The Flisa event epicenter (star) and the stations used for MT inversion (triangles).

The data are filtered by 0.5 – 1.0 Hz. For this event, only an amplitude spectra inversion has been performed so far. Instead of trying to isolate single phases, the wave train is included as a whole. For calculations, the FLISA velocity model by Schweitzer (2005) is used. In Fig. 6.5.13, the misfit-against-depth curve is reproduced.

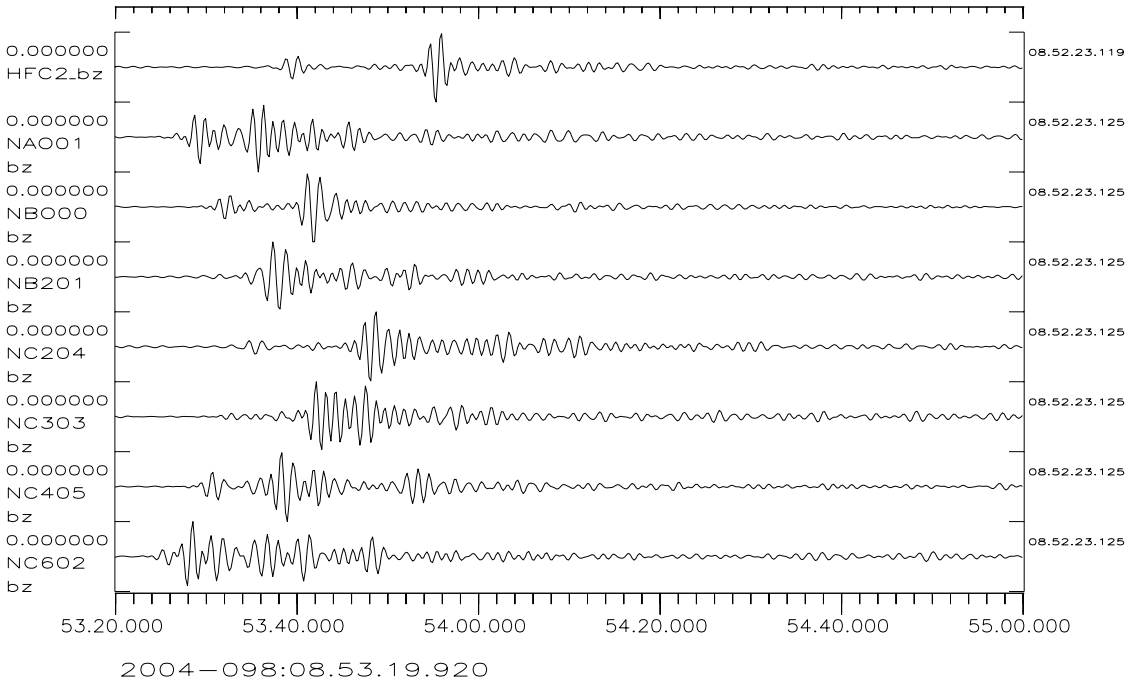

Fig. 6.5.12. Broadband filtered, restituted, resampled and rotated data (filtered by 0.5 – 1.0 Hz).

Two minima can be distinguished, the broader of which is at a depth of 20 km and has a slightly lower misfit of 0.247. The isotropic part amounts to 32% and the DC percentage is 52%. The seismic moment is computed to be 2.2E+14 Nm. The DC solutions are quite stable over a large depth range.

The DC solution given by Schweitzer (2005; Fig. 6.5.14) resulting from polarities of first onsets is extraordinarily constrained by a polarity change of P onsets across the NORSAR array, which is not as clear if one only looks at the broadband stations used for MT inversion. Further, stations from whole Fennoscandia and Estonia were included in the analysis and PmP

polarities at the vertical components of the subarray NC2 were incorporated to restrict the number of possible solutions. These are probably also distinguishable at the central broadband station, but since the seismogram was included as a whole, small amplitudes are attached less importance, so that the PmP onsets might not be of help during an eventual inversion in the time domain.

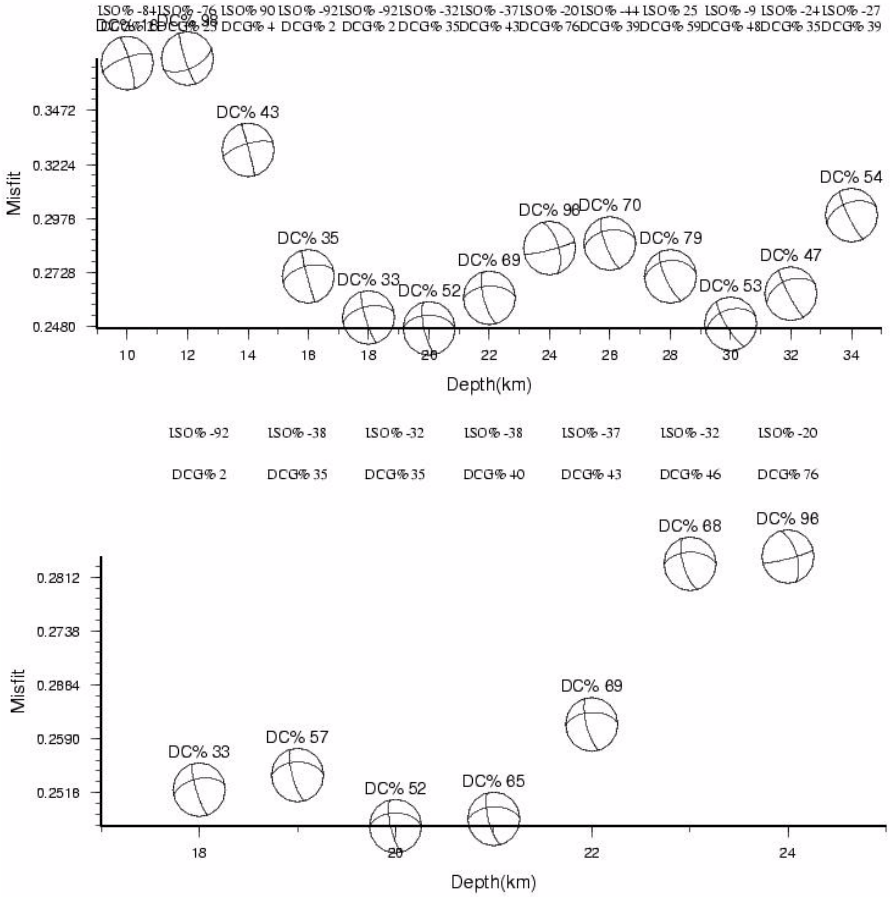

Fig. 6.5.13. Results of the amplitude spectra inversion: misfit and focal solution are plotted against depth; the bottom picture is a cutout of upper graphic.

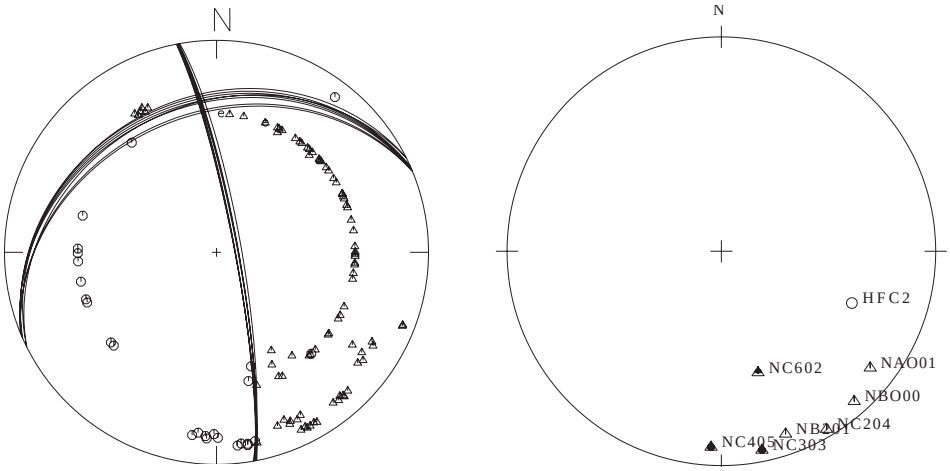

Fig. 6.5.14. Comparison of station distribution; left: stations used by Schweitzer (2005), right: broadband stations available for MT inversion by MTINVERS.

Schweitzer (2005) interprets the steep, north-south striking plane as fault plane consistent with other earthquakes in the Oslo Graben area. The focal depth was determined to be 22.5 km. Fig. 6.5.14 displays a comparison of the station distribution as used by Schweitzer (2005) on the left and the broadband stations available for MT inversion by MTINVERS.

The steep, north-south striking fault plane can be identified as well in the MTINVERS DC solutions. The strike and dip of the auxiliary plane is different, but as can be seen clearly in Fig. 6.5.14, no data were available to constrain its position. Including more stations would clearly improve the solution as well as data from relevant short period stations.

In Fig. 6.5.15, a comparison between observed data and synthetic seismograms is shown. The MT resulting from amplitude spectra inversion is used as source function. Especially for shorter signals, the fit is surprisingly good. Since seismograms have not yet been aligned in time, offsets between both traces can be identified in some cases (*e.g.*, vertical components of NC3 and NC4, radial components of HFC2 and NC3). This may also cause the problem in modelling the radial component of NC4: a wrong cutout which does not even contain the desired signal may have been used for the inversion. In general, the synthetic seismograms tend to be shorter than the observed wave trains, which may be caused by too simple velocity model not correcting for station or scattering effects.

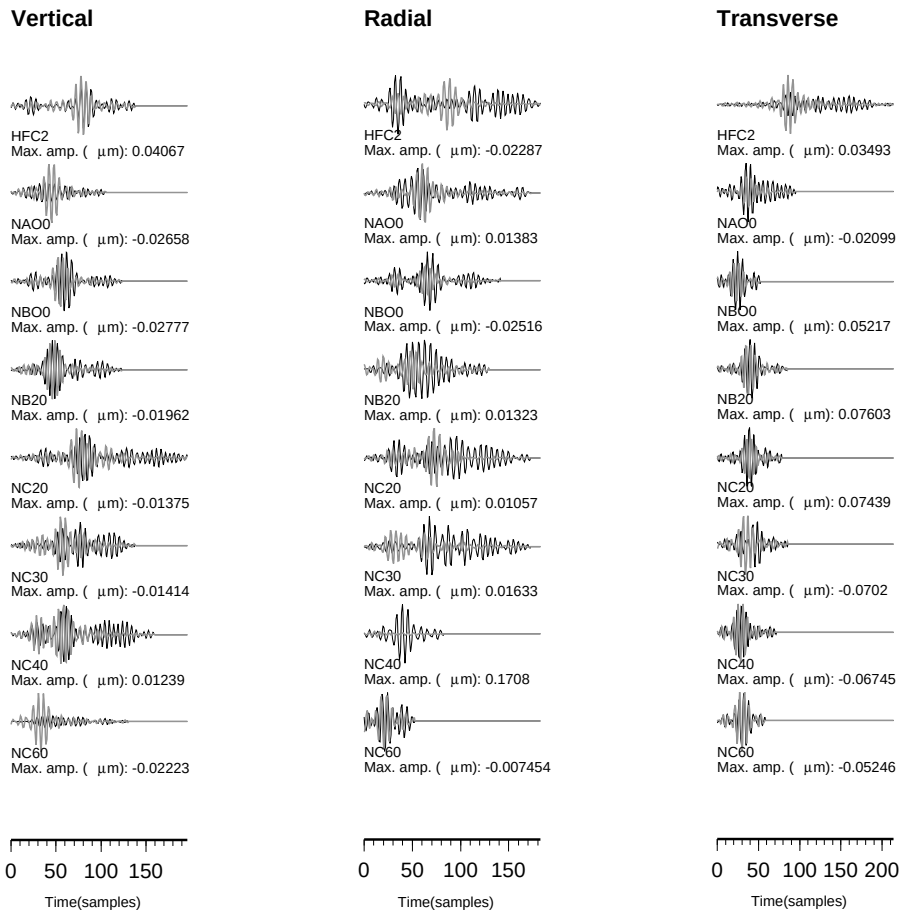

Fig. 6.5.15. Fit between observed data (black lines) and synthetic seismograms (grey lines) with MT source assumed as in Fig. 6.5.13; from left to right: vertical, radial and transverse component.

6.5.5 Conclusions

In general, surprisingly good results were obtained for the regional MT inversion of the 14 April 2004 Jan Mayen and the 04 July 2003 Svalbard event, although the azimuthal coverage is generally not very good when using only regional data directly available at NORSAR. The most critical working step is the alignment of seismograms and Green's functions along with determining the length of the phase analysis window. The longer the phase analysis window, the more information is contained, but at the same time, the risk of overlapping with further phases not aligned correctly in time due to an insufficient velocity model is larger.

The velocity model FESCAN used at first turned out to be too simple for this regional inversion and had to be adjusted by trial-and-error fitting of synthetic to observed seismograms to inprove the modelling of surface wave dispersion.

For regional events, a higher impact in velocity model differences between source and receiver region is noticeable (*e.g.*, oceanic/continental crust, amount of sediments). The larger high-frequency energy content compared to teleseismic events demands a higher accuracy of the velocity model. The oceanic microseismic noise peak in the range of 0.1 – 0.2 Hz overlaps with the body wave frequency spectrum. A judgement of the fit of observed and synthetic seismograms considering the misfit alone is sometimes insufficient (*e.g.,* a bad misfit can be caused by a poor fit at one single station, explainable by an incorrect velocity model). Since the misfit is no objective measure, depending *e.g.,* on time length of the phase analysis window and the frequency content, a comparison to other studies is difficult. Nevertheless, it is a useful tool to compare MT results for individual earthquakes.

In more special cases as that of the 07 April 2004 Flisa event, MT inversions are more difficult. Maybe more stations have to be used to better constrain the auxiliary plane. Even short-period stations may be included, since due to its small size, the high-frequency content of the earthquake is unusually large compared to the Jan Mayen and Svalbard event.

In general, a good velocity model is crucial. It can either be prepared elaborately by incorporating results from other geological or geophysical studies or it can be adapted by hand, which is a very time consuming process.

Another possibility is the application of "pseudo 2-D" velocity models. Raypaths for various source-receiver geometries can be classified in more oceanic or more continental pathways and different 1-D velocity models can be used to calculate the Green's functions for each pair. Besides, other reflectivity codes exist which allow for variable underground models for source and receiver region.

Theoretically, it is possible to apply a 3-D velocity model, but new programs have to be developed. Then, the reflectivity method cannot be applied to compute Green's functions, and *e.g.*, finite-differences or pseudo-spectral codes must be used. MTINVERS has to be adapted, since at the moment, 8 Green's functions are introduced, whereas in the more general 3-D case, 27 Green's functions are required.

Acknowledgments

This project was financially supported by the DAAD (Deutscher Akademischer Austauschdienst, German Academic Exchange Service). Daniela Kühn would like to thank Torsten Dahm and Frank Krüger for e-mail support.

Daniela Kühn, University of Hamburg
Johannes Schweitzer

References

Aki, K. & Richards, P.G. (1980). *Quantitative Seismology: Theory and Methods*. W. H. Freeman and Co., New York, San Francisco.

Backus, G.E. & Mulcahy, M. (1976). Moment tensors and other phenomenological descriptions of seismic sources – I. Continuous displacements. *Geophys. J. R. A. S.*, **46**, 341-361.

Backus, G.E. (1977a). Interpreting the seismic glut moments of total degree two or less. *Geophys. J. R. A. S.*, **51**, 1-25.

Backus, G.E. (1977b). Seismic sources with observable glut moments of spatial degree two. *Geophys. J. R. A. S.*, **51**, 27-45.

Bernardi, F., Braunmiller, J., Kradolfer, U. & Giardini, D. (2004). Automatic regional moment tensor inversion in the European-Mediterranean region. *Geophys. J. Int.*, **157**, 703-716.

Bruhns, C. (2003). *Momententensoren hochfrequenter Ereignisse in Südchile*. PhD Thesis, Universität Potsdam.

Dahm, T. & Krüger, F. (1999), Higher-degree moment tensor inversion using far-field broad-band recordings: theory and evaluation of the method with application to the 1994 Bolivia deep earthquake. *Geophys. J. Int.*, **137**, 35-50.

Dahm, T., Manthei, G. & Eisenblätter, J. (1999). Automated moment tensor inversion to estimate source mechanisms of hydraulically induced micro-seismicity in salt rock. *Tectonophys.*, **306**, 1-17.

Dahm, T., Krüger, F., Stammler, K. & Yuan, X. (2004). Moment tensor inversion – a practical for beginners. ESC Young Scientist Trainings Course, 09-12 September 2004, Potsdam, Germany.

Fyen, J. (2004). *EP – Command Reference and User Guide*. NORSAR.

Gilbert, F. (1973). Derivation of source parameters from low-frequency spectra. *Phil. Trans. Roy. Soc. London*, **A**(274), 369-371.

Harvard CMT catalog (1998). CMT catalog search. Available from World Wide Web: http://www.seismology.harvard.edu, Department of Earth and Planetary Sciences, Harvard University, United Kingdom.

Jost, M.L. & Herrmann, R.B. (1989). A student's guide to and review of moment tensors. *Seis. Res. Lett.*, **60**(2), 37-57.

Kanamori, H. & Given, J. (1981). Use of long-period surface waves for rapid determination of earthquake-source parameters. *Phys. Earth Plan. Int.*, **27**, 8-31.

Knopoff, L. & Randall, M.J. (1970). The compensated linear-vector dipole: a possible mechanism for deep earthquakes. *J. Geophys. Res.*, **75**, 4957-4963.

Krüger, F. & Dahm, T. (2002). The 1992 Roermond earthquake, a regional event study. In Senate Commission for Geoscience, Editor, *Ten Years of German Regional Seismic Network (GRSN)*, Report 25, DFG.

Müller, G. (1985). The reflectivity method: a tutorial. *J. Geophys. Res.*, **58**, 153-174.

Roth, M. & Bungum, H. (2003). Waveform modeling of the 17 August 1999 Kola Peninsula earthquake. *Bull. Seis. Soc. Am.*, **93**(4), 1559-1572.

Schweitzer, J. (2005). The 7 April 2004 Flisa, Southern Norway earthquake sequence – eight hypocenter determinations and one focal mechanism. *NORSAR Sci. Rep.*, **1-2005**, 62-76.

Sipkin, S.A. (1982). Estimation of earthquake source parameters by the inversion of waveform data: synthetic waveforms. *Phys. Earth Plan. Int.*, **30**, 242-255.

Stange, S. & Schweitzer, J. (2004). Source depths at regional distances: an example from the Western Barents Sea/Svalbard Region. *NORSAR Sci. Rep.*, **1-2004**, 45-50.

Stein, S. & Wysession, M. (2003). *An Introduction to Seismology, Earthquakes and Earth Structure*. Blackwell Publishing.

Ungerer, J. (1990). Berechnung von Nahfeldseismogrammen mit der Reflektivitätsmethode. Institut für Geophysik, Universität Stuttgart. Diplomarbeit.

Wessel, P. & Smith, W.H.F. (2003). *GMT – Technical Reference and Cookbook*. School of Ocean and Earth Science and Technology. Version 3.4.3.